Interstellar dust and polycyclic aromatic hydrocarbons unveiled by *AKARI* near-infrared spectroscopy

JI YEON SEOK[1]

[1]*Key Laboratory of Optical Astronomy, National Astronomical Observatories, Chinese Academy of Sciences, Beijing 100012, China*

ABSTRACT

Spectral features from gas and dust in the various interstellar environment residing at 2 to 5 μm have been unveiled thanks to high-sensitivity spectroscopy achieved by the infrared camera (IRC) on board *AKARI*. The well-known emission feature at 3.3 μm, commonly attributed to polycyclic aromatic hydrocarbons (PAHs) as well as other minor features such as the aliphatic emission band at 3.43 μm were detected from diverse physical conditions, including H II regions, supernova remnants, and starburst galaxies. These features are also commonly observed in protoplanetary disks (PPDs) around Herbig Ae/Be and T Tauri stars over wide evolutionary phases. The aromatic/aliphatic features are often used as a diagnostic tool of the physical and chemical conditions of their surroundings. In this review, the key contributions made by *AKARI* near-infrared spectroscopy are discussed with special attention paid to the interstellar dust and PAHs.

Keywords: ISM

1. INTRODUCTION

Gas and dust in the interstellar medium (ISM) emanate a significant fraction of their energy through spectral features at infrared (IR) wavelengths. In particular, a distinct set of broad emission feature at 3.3, 6.2, 7.7, 8.6, and 11.2 μm, collectively known as unidentified infrared (UIR) emission bands, are ubiquitously seen in a wide range of astrophysical objects including young stellar objects, H II regions, the diffuse ISM, and starburst galaxies. UIR bands are commonly attributed to polycyclic aromatic hydrocarbons (PAHs; Léger, A., & Puget 1984; Allamandola et al. 1985). Thus, infrared observations enable us to examine the processing of dust and PAHs most efficiently.

The 2 to 5 μm wavelength range contains unique information on the nature of the ISM. There is a major UIR feature at 3.3 μm, which often accompanies substructures at $\sim$ 3.4–3.6 μm. The 3.3 μm feature is commonly attributed to aromatic C-H stretching vibrations while the 3.4 μm feature is due to C-H vibrations of aliphatic hydrocarbons (Joblin et al. 1996, see more in Section 4). In addition, hydrogen recombination lines at 2.626, 3.297, 3.741, 4.052, and 4.654 μm, molecular hydrogen lines (e.g., 1-0 O(3), O(5), and 0-0 S(9) at 2.803, 3.235, and 4.695 μm, respectively), various ice features (e.g., H_2O and CO_2 ice absorption at 3.0 and 4.3 μm), and nanodiamond features at 3.4 and 3.5 μm exist in the spectral range of 2–5 μm (e.g., Acke & van den Ancker 2006; Shimonishi et al. 2008; Seok et al. 2012; Mori et al. 2014, and also see Figures 1–3). Despite of its importance, the near-infrared (NIR) band shorter than 5.5 μm has not been fully explored due to lack of the observational data compared to longer wavelengths. Among the previous IR space missions such as the *IRAS*, *ISO*, and *Spitzer*, the SWS spectrometer on board the *ISO* was capable of performing spectroscopic observations at this spectral range, but very bright sources were mostly targeted due to its sensitivity. The Infrared Camera (IRC) onboard *AKARI* (Murakami et al. 2007) enables us to carry out sensitive spectroscopy in the NIR (Onaka et al. 2007), which significantly improve our understanding of the spectral features appearing in this NIR range. Furthermore, the upcoming *James Webb Space Telescope (JWST)* will offer a continuous spectral coverage from the optical to the mid-infrared (MIR; 0.6–28.3 μm) with various resolving powers. Since the *JWST* is going to launch in the near future, it is necessary for us to review the important *AKARI* contributions to our understanding of dust and PAHs revealed by the NIR spectroscopy and consider to make synergy with them for future science.

In the following, several observational results achieved by the IRC NIR spectroscopy are highlighted focusing on dust and PAHs in the ISM. Also, PAHs in protoplanetary disks (PPDs) are discussed together with preliminary results obtained with *AKARI* IRC spectra.

Corresponding author: Ji Yeon Seok
jiseok@bao.ac.cn

2. *AKARI* NIR SPECTROSCOPY

The Japanese infrared satellite, *AKARI* (Murakami et al. 2007), has capabilities in imaging and spectroscopy from near-infrared (NIR) to far-infrared (FIR) wavelengths, which has provided rich data sets for us to investigate comprehensively the nature of dust as well as gas in the ISM. The IRC on board *AKARI* is composed of three channels (NIR, MIR-S, and MIR-L) covering 1.8–26.5 μm (Onaka et al. 2007). The IRC provides a unique opportunity to perform high-sensitivity spectroscopy at the NIR wavelengths ($\sim$ 2 to 5 μm) for the first time from space. Even after the exhaustion of the liquid helium (i.e., the post-He phase), the NIR channel continued to operate with its high sensitivity retained (Onaka et al. 2010). There are three types of slits available for NIR spectroscopy with prism (NP, low-resolution: $R \sim 20$–40) and/or grism (NG, high-resolution: $R \sim 100$): $1'$ by $1'$ wide slit designed for the spectroscopy of point sources with a grism (NG;Np) and two slits (Ns: $5'' \times 0.''8$ with both prism and grism, Nh: $3'' \times 1'$ for the highest spectral resolution ($R \sim 150$) with a grism) for diffuse sources (see Figure 3 in Onaka et al. 2007). In addition to slit spectroscopy, the IRC has the unique capability to perform slit-less spectroscopy, which offers multi-object spectroscopy from the NIR to MIR.

3. DUST PROCESSING IN SUPERNOVA REMNANTS

As a result of a supernova (SN) explosion, a significant amount of dust grains may be formed in the SN ejecta (e.g., Matsuura et al. 2011; Indebetouw et al. 2014) while SN shocks heat and accelerate the ambient medium and destroy dust grains in the ISM. These competing processes can be studied by observing supernova remnants (SNRs) at various wavelengths, most efficiently, at infrared wavelengths.

Rho et al. (2012) detected carbon monoxide (CO) emission from SN eject in the young core-collapse SNR Cassiopeia A (Cas A) using the *AKARI* NIR slit spectroscopy. The NIR spectra obtained toward several positions in Cas A including shocked and unshocked SN ejecta unambiguously show the double-peaked profile indicative of the unresolved ro-vibrational band due to the CO fundamental at 4.65 μm (see their Figure 1 in Rho et al. 2012). The presence of CO in the unshocked ejecta at the center reveals that CO molecules form in the ejecta at an early phase. The detection of CO emission from the shocked ejecta demonstrates that a significant portion of the CO molecules has survived for at least $\sim$ 330 years after the initial SN explosion, indicating inefficient destruction of CO in Cas A. This result implies that significant amounts of carbon may have been locked in CO, which gives an important implication for dust formation in SNe that less carbon is available to form carbonaceous dust in SNe than what is currently thought.

Interstellar shocks are considered to play a key role in processing PAHs in the ISM. SN shocks are one of the primary mechanisms that alter and destroy PAH molecules. In addition to the formation of PAHs in asymptotic giant branch star, the fragmentation of carbonaceous grains through a shattering collision in fast interstellar shocks can contribute to form PAHs (e.g., Jones et al. 1996; Seok et al. 2014). In this context, studying PAHs in SNRs is ideal to examine PAH processing in SN shocks although confusion with PAHs in background emission makes it complicated in practice. So far, PAH emission bands associated with the remnant have been detected from only handful of SNRs in the Large Magellanic Cloud (LMC) as well as the Milky Way (e.g., Tappe et al. 2006; Rho et al. 2011; Seok et al. 2012). Since it is located away from the Galactic disk, the LMC could be one of the best places to observe the PAH emission from SNRs avoiding serious confusion from Galactic sources. The middle-aged, bright LMC SNR N49 exhibits the 3.3 μm aromatic feature together with other emission lines in its NIR (2–5 μm) spectra obtained with *AKARI* (Seok et al. 2012, see Figure 1 therein), which is the first time that the detection of the 3.3 μm feature in SNRs has been reported.

As a coarse spectral mapping, fourteen spectra were taken to cover a large area of N49 focusing on a bright wedge-shaped feature in the east. This bright east region is where the SNR interacts with the ambient molecular cloud (Banas et al. 1997), and the 3.3 μm feature is detected most strongly in this region. Since the 3.3 μm feature mainly arises from relatively small PAHs due to C–H stretching mode, the detection of the 3.3 μm feature in N49 is indicative of the presence of small PAHs in the SNR. In addition to the IRC spectra, the MIR spectra from the *Spitzer* archive suggest that PAHs in N49 are not only small in size but also dominantly neutral based on the relative strengths of the PAH bands (i.e., 6.2, 7.7, and 11.3 μm bands). This indicates that even small, neutral PAHs can survive against complete destruction by SN shocks, and for the survival of PAHs in shock regions, an ambient dense medium such as dense clumps is needed (Micelotta et al. 2010). Moreover, although PAHs can survive a slow shock, strong PAH emission may not arise due to the lack of UV radiation. Hence, a sufficient heating source is also required for PAHs to radiate in SNRs.

4. AROMATIC AND ALIPHATIC FEATURES AT 3.3–3.6 μm

The UIR band near 3 μm exhibits a rich, complex spectrum, observed frequently in Galactic H II regions, reflection nebulae, and planetary nebulae, in the general ISM as well as in a number of extragalactic sources (e.g., Imanishi et al. 2010). The well-known 3.3 μm UIR band, attributed to C–H stretching vibrations of aromatic hydrocarbons, is often accompanied with a weaker emission at 3.4 μm together with an underlying plateau extending up to $\sim$ 3.6 μm. In addition to these features, a series of weaker emission at 3.46, 3.51, and 3.56 μm appear in some objects (e.g., Sloan et al. 1997). Unlike the 3.3 μm emission feature, the precise assignment of the 3.4 μm feature and other minor features at 3.4–3.6 μm still remains somewhat controversial. The 3.4 μm feature is often considered due to the C–H vibrational modes in aliphatic hydrocarbons (e.g., Joblin et al. 1996; Chiar et al. 2000; Pendleton & Allamandola 2002; Yang et al. 2016) although anharmonicity and/or superhydrogenation of the aromatic C–H stretch can also contribute to this feature (Baker

et al. 1987; Bernstein et al. 1996). Adopting that the 3.4 μm feature is exclusively due to aliphatic hydrocarbons, the intensity of the 3.4 μm band relative to that of the 3.3 μm can constrain the aliphatic fraction of the UIR band carriers.

With *AKARI*, Yamagishi et al. (2012) obtained NIR spectra of 34 regions in the nearby starburst galaxy, M82, which shows prominent galactic superwind. The *AKARI* NIR spectra were taken from the whole galaxy including the center, disk, and halo regions, and many of them show the 3.3 μm feature together with the weaker features at 3.4–3.6 μm. It is previously known that the PAH emission is extended to the halo (Engelbracht et al. 2006), but it was the first time to show the presence of the 3.3 μm emission in the halo spectroscopically. The relative strength of the subfeatures at 3.4–3.6 μm to the 3.3 μm feature varies with positions in M82. Attributing the subfeatures to aliphatic hydrocarbons, Yamagishi et al. (2012) derived the ratio of the aliphatic features to the total excess (i.e., the integrated intensity of the aromatic and aliphatic emission) and correlated them with the distance from the center of M82 (see their Figure 3). The ratio tends to increase with the distance from the galactic center, indicating that the strength of the aliphatic features relative to the aromatic feature is enhanced in the halo. In fact, several spectra from the halo regions show that the 3.4–3.6 μm emission becomes even stronger than the 3.3 μm feature. This unusually strong aliphatic feature in the halo implies that fragmentation of larger grains into small carbonaceous ones emitting the aliphatic features occurs in shocks. Meanwhile, the presence of the 3.3 μm feature in the halo indicates that small PAHs are considerably protected in dense molecular clouds against preferential destruction by shocks.

In addition to fragmentation in shocks, the production of PAHs from very small grains (VSGs) in photon-dominate regions (PDRs) through evaporation under UV irradiation has been proposed (e.g., Jones 2012). Pilleri et al. (2015) examined the evolution of aliphatic and aromatic CH groups in the prototypical PDR NGC 7023 with *AKARI* and *Spitzer* data. They measured the ratio of the 3.4 μm to 3.3 μm features, which decreases largely at the PDR layers exposed to strong UV radiation. In particular, the 3.4/3.3 μm ratio peaks close to the regions where VSGs are photo-evaporated into PAHs. This supports that the photo-processing of evaporating VSGs can contribute the formation of PAHs with attached aliphatic sidegroups. In addition, the intensity of the 3.4 μm feature relative to the total neutral PAH intensity tends to decrease with the radiation field intensity, indicating that their carriers are efficiently destroyed by UV irradiation.

5. PAH FEATURE AT 5.25 μm

In addition to the major UIR bands at 3.3, 6.2, 7.7, 8.6, and 11.2 μm, there is a variety of minor UIR bands such as weaker features at 3.4, 3.5, 5.25, and 5.75 μm, which appear at certain types of astronomical objects reflecting the local physical conditions (Tielens 2008). It is thus important to investigate the nature of these minor UIR bands and to correlate them with the local environment. Mori et al. (2014) have collected a large set of *AKARI* NIR spectra of Galactic H II regions and H II region-like objects to carry out a systematic study of PAH features in these objects. They found that most spectra show the well known 3.3–3.6 μm features due to aromatic and/or aliphatic hydrocarbons as well as a relatively weak emission feature at 5.22 μm, which can be identified as the PAH 5.25 μm band (Allamandola et al. 1989). Previously, this feature is attributed to a blend of overtone, difference, and combination bands of the fundamental C–H stretching and bending vibrational modes (Allamandola et al. 1989). Because of its weakness as well as the lack of observational data, however, a comprehensive analysis has not been carried out. Mori et al. (2014) compared the intensity of the 5.25 μm feature with those of the 3.3 μm aromatic feature and the 3.4–3.6 μm subfeatures and found that both show a tight correlation (see their Figure 4). This implies that the 5.25 μm band is physically associated with C–H vibrational modes. Moreover, the 5.25 μm band shows a slightly better correlation with the 3.3 μm band, which indicates that the carrier of 5.25 μm feature is more likely to be aromatic ones.

This detailed study of the 5.25 μm feature was made possible thanks to the wide wavelength coverage of the prism mode (1.8–5.5 μm; Onaka et al. 2007). In near future, the *JWST* will provide a continuous spectral coverage from the optical to the MIR (0.6–28.3 μm)[1], and the 5.25 μm band is expected to be seen as frequently as the major UIR bands from a wide range of astronomical objects. Considering that the ratio of the 3.3 μm to 11.2 μm bands is often used as a probe of PAH size, the tight correlation between the 5.25 μm and 3.3 μm features suggests that the 5.25 μm feature can be also used as a diagnostic tool for studying the size of PAH molecules. Therefore, more data from the *JWST* complemented with the *AKARI* data will shed new light on the true nature of the 5.25 μm feature as well as its correlations with other UIR bands.

6. DEUTERATED PAHS

The amount of deuterium (D) in a galaxy provides a direct measure of cosmic nucleosynthesis, which tells us about the chemical evolution of the galaxy itself (Epstein et al. 1976). Previously, deuterium-enriched PAHs (PADs; Hudgins et al. 2004) have been suggested as a potential reservoir of D in the ISM (Draine 2006). When hydrogen in PAHs is replaced by D, the C-D vibrational modes are supposed to move to longer wavelengths relative to the corresponding C-H vibrational modes due to the heavier mass of D. For instance, the well-known aromatic C–H stretching mode at 3.29 μm is shifted to 4.40 μm with the aromatic C–D stretching mode. Similarly, C–H aliphatic features at 3.40 and 3.50 μm fall at 4.63 and 4.75 μm for C–D, respectively.

Onaka et al. (2014) obtained spectra of the Orion Bar and M17 where detection of PADs (primarily C–D asymmetric stretching feature) have been previously reported (Verstraete et al. 1996; Peeters et al. 2004) based on observations with

---

[1] https://jwst.stsci.edu/instrumentation

the short wavelength spectrometer (SWS) on board the *Infrared Space observatory (ISO)*. After the subtraction of line emission from the ionized gas, neither of the spectra of the Orion Bar nor M17 shows significant excess emission is found in 4.3–4.7 μm in the spectra. They put an upper limit for the PAD/PAH ratio of $\sim$ 3% at most, which is an order of magnitude smaller than the previous results as well as the model prediction (D/H ratios in PAHs $\sim$ 0.3; Draine 2006). In addition, the PAD features are also searched for the reflection nebula GN 18.14.0, which does not require the subtraction of the ionized gas emission thanks to their absence in the range 4–5 μm. Similarly, GN 18.14.0 also gives the PAD/PAH intensity ratio of about 2% if excess emission in the 4 μm region due to PADs is present.

Later, Doney et al. (2016) revisited PADs with a larger number of samples from *AKARI*. They obtained NIR spectra of 53 H II regions in the Milky Way and the Large and Small Magellanic Clouds, which include 33 Galactic objects from Mori et al. (2014). Only six out of the 53 objects show excess emission due to PADs, all of which are located in the Milky Way. Both Onaka et al. (2014) and Doney et al. (2016) conclude that the mechanisms for PAH deuteration in the ISM is uncommon. However, Doney et al. (2016) suggest that although dueterated PAHs are not omnipresent, when present, dueteration is efficient. They found that all measured PAH D/H ratios from the six objects are significantly larger (ranging from $\sim$ 0.03 to 0.44) than the cosmic gas-phase abundance of $\sim 10^{-5}$ (Vidal-Madjar et al. 1998). Thus, PAHs can still explain the variation of the galactic gas-phase D/H ratio to some extent.

7. PAHS IN PROTOPLANETARY DISKS

PAH molecules are thought to play important roles in disk physics and chemistry. In the upper layer of a disk, free-flying PAHs are directly exposed to UV (and visible) photons from a central star and get ionized efficiently. Photoelectrons from these PAHs are the primary heating source of gas in the disk, which, in turn, influence thermal processes occurring in the disk (e.g., Kamp & Dullemond 2004). PAHs offer large surface areas for chemical reactions (e.g., Habart et al. 2004), and in particular, PAHs can alter carbon chemistry via electron transfer. Moreover, PAHs can be associated with very small grains (VSGs) in the disk, which infer dust processing such as settling and coagulation. Because these processes are crucial to form planetesimals, PAHs can affect the early phase of planet formation.

Disks around low- and intermediate-mass pre-main-sequence stars often exhibit the PAH emission in their IR spectra (e.g., Meeus et al. 2001; Habart et al. 2004; Geers et al. 2007; Keller et al. 2008; Acke et al. 2010; Maaskant et al. 2014; Seok & Li 2016). According to *Spitzer* observations, about 70% of disks around Herbig Ae/Be stars (HAeBe) with a stellar mass of 2–8 $M_\odot$ clearly show PAH features in their spectra (Acke et al. 2010), while less than 10% of the disks around T Tauri stars (TTSs; $\lesssim 2M_\odot$) show PAH emission (e.g., Furlan et al. 2006). These results indicate that the absence or presence of PAH emission in the protoplanetary disks (PPDs) seems to correlated with the stellar properties and evolution of the disks. In addition to the detection rate of PAH emission, spectral variations among PAH features have been reported among PPDs with different stellar properties (e.g., Keller et al. 2008), which suggest the PAH features can be used as a diagnostic tool of the physical conditions of PPDs and a tracer of disk structure. Therefore, it is desirable to perform a systematic study about PAHs in PPDs with a large number of samples covering a wide range of stellar parameters such as effective temperature, stellar mass, and stellar age.

We investigate PAH emission in PPDs with a large number of sample (Seok & Li 2017): 69 PPDs with IR spectra showing PAH emission are collected in the literature, including 14 TTSs and 55 HAeBe stars. The data consist of IR spectra obtained with the *ISO*, *Spitzer*, as well as several ground-based telescopes such as the NASA Infrared Telescope Facility (IRTF), Very Large Telescope (VLT), and ESO La Sila Observatory. Unfortunately, *AKARI* data are not used in this work because no data hasn't been published in the literature so far although spectroscopic observations have been performed toward several objects in the sample (see 7.1). To derive physical properties of PAHs in PPDs, we model the PAH emission features in terms of astronomical PAHs. We adopt the astro-PAH model of Li & Draine (2001b) and Draine & Li (2007), assuming a log-normal distribution function (dn_{PAH}/da) for the PAH size. The size distribution is determined by the peak (a_0) and the width (σ) of the log-normal function. Using dn_{PAH}/da, the peak of the mass distribution (a_p) is calculated (Li & Draine 2001a). We quantify the charge state of PAHs in PPDs by varying the ionization fraction (ϕ_{ion}), which is the probability of finding a PAH molecule in a nonzero charge state (Li & Lunine 2003).

Based on the best-fit model, we examine correlations between PAH properties and stellar parameters. The stellar effective temperature (T_{eff}), one of the key environmental factors, tends to positively correlate with the peak size of the PAH size distribution (a_p). This correlation can be readily explained: because photons from the central sources with a high T_{eff} are more energetic, small PAHs are likely to be destroyed preferentially due to photodissociation. For ϕ_{ion}, on the other hand, it does not show any correlation with T_{eff}. This might be attributed to the diversity of the spatial distribution of PAHs among PPDs. To interpret ϕ_{ion} correctly, the spatial distribution of PAHs in a disk should be taken into account.

7.1. Preliminary results of PPDs with *AKARI*

Note that it is important to use a spectrum covering a wide spectral range (i.e., $\sim$ 3–20 μm) in order to include all major PAH bands because a simultaneous modeling of as many PAH bands as possible can constrain PAH properties more precisely. Due to observational constraints, however, spectra at wavelengths shorter than 5 μm are available only for bright sources from ISO and/or ground-based telescopes. Previously, Acke & van den Ancker (2004) surveyed 46 disks around HAeBe stars with ISO. PAH bands are detected from roughly a half of their sample, and a small minority of stars (e.g., HD 97048, V892 Tau) also display nanodiamond-related features at 3.4 and 3.5 μm.

To further examine PAH emission from PPDs at short wavelengths ($\lesssim 5~\mu$m), we have searched the *AKARI* archive[2] for NIR spectra of PPDs. About 20 out of 69 PPDs in the sample of Seok & Li (2017) have been observed by *AKARI*/IRC spectroscopically. After retrieval of data from the archive, the data reduction was carried out with the official pipeline optimized for Phase 3 version 20150331. Among the targets, six sources (IRAS 03260+3111, V892 Tau, HD 97048, HD 97300, TY CrA, and BD+40°4124) clearly exhibit PAH emission as well as other minor features, and their preliminary spectra are presented in Figures 1–3. Moreover, HD 97048 and V892 Tau (a.k.a. Elias 3-1) show strong nanodiamond features in the IRC spectra as reported previously (see Figure 3). Observational details for the six sources are listed in Table 1.

Table 1. Journal of the Observations

Source	Slit	α(J2000.0)	δ (J2000.0)	Pointing ID	Observation Date
IRAS 03260+3111	Ns	3:29:10.43	+31:21:59.8	1420767.1	2008-08-20
V892 Tau	Ns	4:18:40.59	+28:19:15.2	1420769.1	2008-08-30
HD 97048	Ns	11:08:03.32	-77:39:17.5	1420765.1	2008-08-22
HD 97300	Np	11:09:50.02	-76:36:47.7	1640162.1	2008-08-19
TY CrA	Ns	19:01:40.83	-36:52:33.9	1420761.1	2009-04-01
BD+40°4124	Ns	20:20:28.25	+41:21:51.6	1420759.1	2008-11-15
	Ns	20:20:28.25	+41:21:51.6	1420760.1	2008-11-17

Since all six objects have been previously observed by *ISO*, the IRC spectra are compared with the *ISO* spectra, which show good agreement with each other. For HD 97300, the 3.3 μm PAH emission is clearly seen in the IRC spectrum unlike the ISOPHOT spectrum that barely shows the feature owing to the low signal-to-noise ratio (Figure 1(a)). There are two IRC spectra available for BD+40°4124 as shown in Figure 1(c). Although their continuum levels are slightly different probable due to inconsistent positions of the source on the slit (Ns slit with a width of 5″), the spectral features shown in both spectra are consistent with each other. In addition to the prominent 3.3 μm feature, the 3.4 μm aliphatic feature with an additional broad emission peaking at 3.45 μm, often referred to as the plateau, is clearly detected, which is not previously seen in the *ISO*/SWS spectrum. TY CrA is a quadruple system (Chauvin et al. 2003), which is surrounded by a nebulosity including a bar-like structure revealed in the IR images (e.g., Boersma et al. 2009). The emission from the nebulosity is most likely to dominate its *ISO*/SWS spectrum with a large aperture (e.g., Geers et al. 2007). Using the IRC spectrum, we extract the emission from the nebulosity separately and subtract the total spectrum by the nebular spectrum (Figure 2). The residual spectrum represents the emission from the disk of TY CrA, which does not have the strong aliphatic emission at 3.4–3.5 μm. This is consistent with the spatially resolved spectrum obtained with the ISAAC instrument installed at the VLT (Geers et al. 2007). Although the six objects have been observed previously, we can identify several new emission features from the preliminary IRC spectra, which can improve our understanding on PAH processing in these systems.

8. FUTURE PERSPECTIVE

NIR spectroscopy at the wavelength range of 2–5 μm is a unique capability of *AKARI*. In particular, a number of spectroscopic observations at this spectral range have been carried out during the post-He Phase (Phase 3). Now all the *AKARI* observations have been reprocessed, and most of final data products can be found from the archive. The upcoming *JWST* will offer significantly higher spectral resolution in the NIR range (1–5 μm): for example, the Near Infrared Spectrograph (NIRSpec) has low, medium, and high spectral resolutions (R = 100, 1000, and 2700, respectively) at 0.6–5.3 μm. In addition, the multi-object spectroscopy as well as integral field unit are also available. Future observations from the *JWST* (and other ground-based IR telescopes) combined with the existing data from *AKARI* will greatly improve our understanding on the interstellar dust and PAHs.

ACKNOWLEDGMENTS

---

[2] http://www.ir.isas.jaxa.jp/AKARI/Archive/

(a) HD 97300

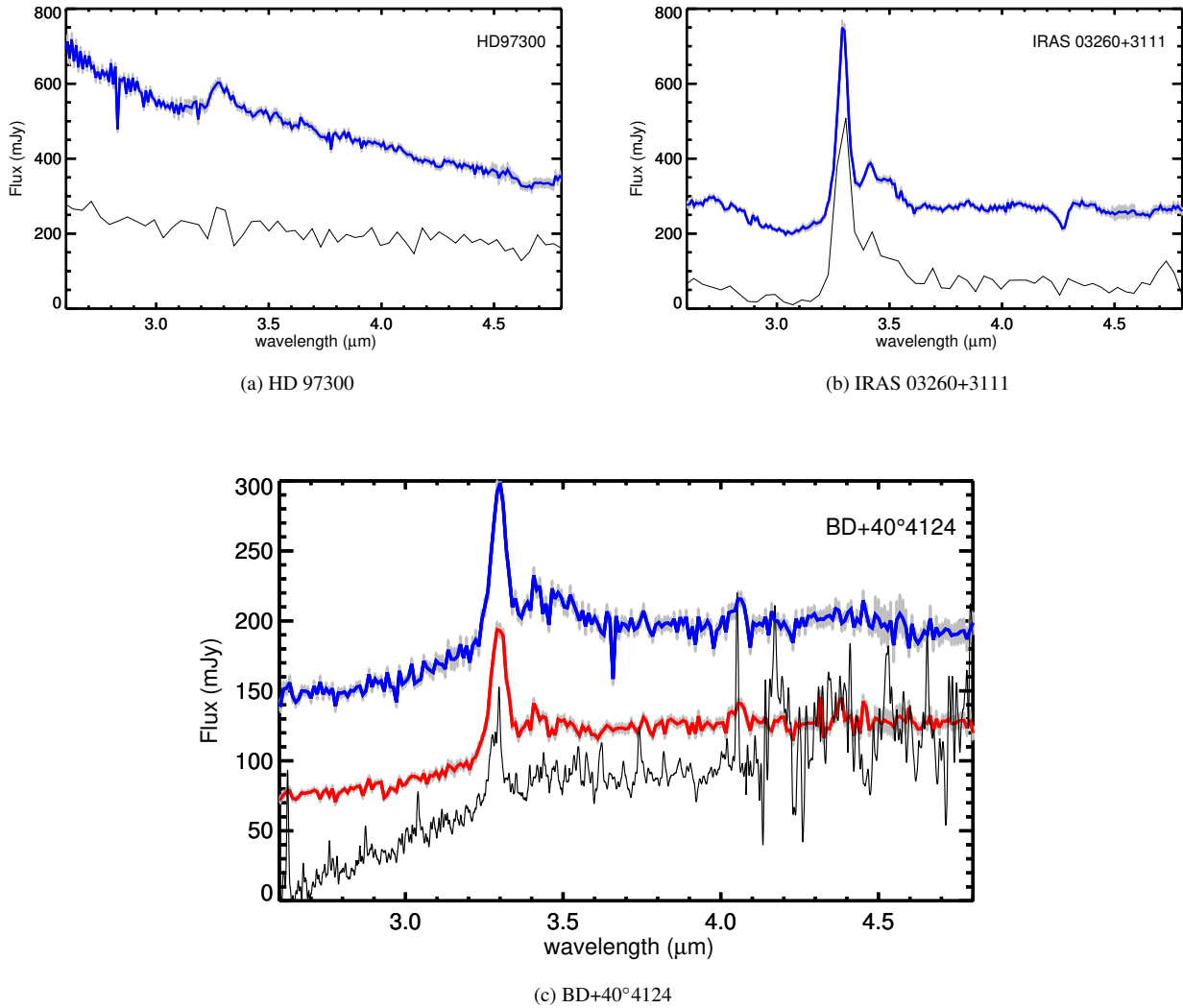(b) IRAS 03260+3111

(c) BD+40°4124

Figure 1. *AKARI* IRC spectra of (a) HD 97300, (b) IRAS 0320+3111, and (c) BD+40°4124 shown in blue lines. For BD+40°4124, two *AKARI* spectra are presented (blue: 14207259.1, red: 1420760.1, see Table 1). Uncertainties from the pipeline are shown in grey. For comparison, (scaled and shifted) *ISO* spectra (ISOPHOT for HD97300 and IRAS 03260+3111, SWS for BD+40°4124) are overlaid with black lines.
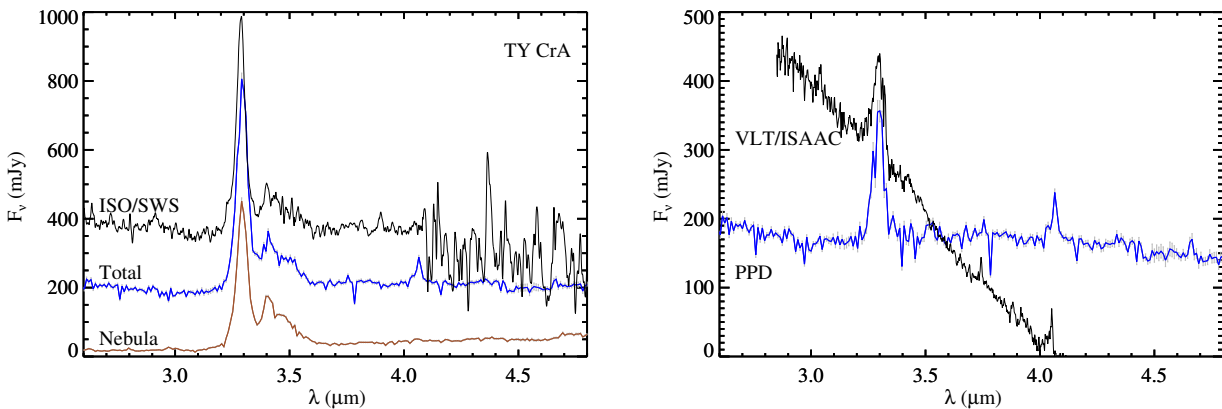

Figure 2. IRC spectra of TY CrA. As TY CrA has extended nebulosity, the total and nebula spectra (blue and brown lines, respectively) are extracted (left panel). For comparison, a *ISO*/SWS spectrum is shown, too. After subtracting the total spectrum by the nebular, the spectrum of the PPD is obtained (right panel), which is compared to the VLT/ISAAC spectrum from (Geers et al. 2007).
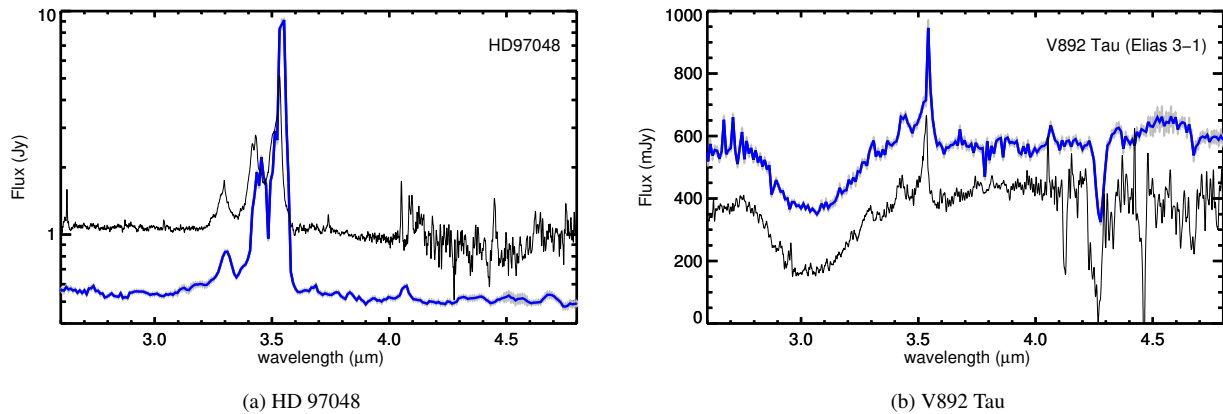
(a) HD 97048

(b) V892 Tau

Figure 3. (a) HD 97049 and (b) V892 Tau (a.k.a. Elias 3-1) with a prominent nano-diamond feature at 3.5 μm. *AKARI* IRC spectra are shown in blue while (scaled and shifted) *ISO*/SWS spectra are in black for comparison.

REFERENCES

Acke, B., & van den Ancker, M. E. 2004, A&A, 426, 151
Acke, B., & van den Ancker, M. E. 2006, A&A, 457, 171
Acke, B., Bouwman, J., Juhász, A., et al. 2010, ApJ, 718, 558
Allamandola, L. J., Tielens, A. G. G. M., & Barker, J.R. 1985, ApJ, 290, L25
Allamandola, L. J., Tielens, A. G. G. M., & Barker, J. R. 1989, ApJS, 71, 733
Barker, J.R., Allamandola, L.J., & Tielens, A.G.G.M. 1987, ApJ, 315, L61
Banas, K. R., Hughes, J. P., Bronfman, L., & Nyman, L.-A. 1997, ApJ, 480, 607
Bernstein, M.P., Sandford, S.A., & Allamandola, L.J. 1996, ApJ, 472, L127
Boersma, C., Peeters, E., Martín-Hernández, N. L., et al. 2009, A&A, 502, 175
Chauvin, G., Lagrange, A.-M., Beust, H., et al. 2003, A&A, 406, L51
Chiar, J. E., Tielens, A. G. G. M., Whittet, D. C. B., et al. 2000, ApJ, 537, 749
Doney, K. D., Candian, A., Mori, T., Onaka, T., & Tielens, A. G. G. M. 2016, A&A, 586, A65
Draine, B. T. 2006, in ASP Conf. Ser. 348, Proc. Astrophysics in the Far Ultraviolet: Five Years of Discovery with FUSE, ed. G.
    Sonneborn, H. Moos, & B.-G. Andersson (San Francisco, CA: ASP), 58
Draine, B.T., & Li, A. 2007, ApJ, 657, 810
Engelbracht, C. W., Kundurthy, P., Gordon, K. D., et al. 2006, ApJL, 642, L127
Epstein, R. I., Lattimer, J. M., & Schramm, D. N. 1976, Nature, 263, 198
Furlan, E., Hartmann, L., Calvet, N., et al. 2006, ApJS, 165, 568
Geers, V. C., van Dishoeck, E. F., Visser, R., et al. 2007, A&A, 476, 279
Habart, E., Natta, A., & Krügel, E. 2004, A&A, 427, 179
Hudgins, D. M., Bauschlicher, C. W., Jr., & Sandford, S. A. 2004, ApJ, 614, 770
Imanishi, M., Nakagawa, T., Shirahata, M., Ohyama, Y., & Onaka, T. 2010, ApJ, 721, 1233
Indebetouw, R., Matsuura, M., Dwek, E., et al. 2014, ApJL, 782, L2
Joblin, C., Tielens, A.G.G.M., Allamandola, L.J., & Geballe, T.R. 1996, ApJ, 458, 610
Jones, A. P., Tielens, A. G. G. M., & Hollenbach, D. J. 1996, ApJ, 469, 740
Jones, A. P. 2012, A&A, 542, A98
Kamp, I., & Dullemond, C. P. 2004, ApJ, 615, 991
Keller, L. D., Sloan, G. C., Forrest, W. J., et al. 2008, ApJ, 684, 411
Léger, A., & Puget, J. 1984, A&A, 137, L5
Li, A., & Draine, B.T. 2001a, ApJ, 550, 213
Li, A., & Draine, B.T. 2001b, ApJ, 554, 778
Li, A., & Lunine, J. I. 2003, ApJ, 594, 987
Maaskant, K. M., Min, M., Waters, L. B. F. M., & Tielens, A. G. G. M. 2014, A&A, 563, A78
Matsuura, M., Dwek, E., Meixner, M., et al. 2011, Science, 333, 1258
Meeus, G., Waters, L. B. F. M., Bouwman, J., et al. 2001, A&A, 365, 476
Micelotta, E. R., Jones, A. P., & Tielens, A. G. G. M. 2010, A&A, 510, A36
Mori, T. I., Onaka, T., Sakon, I., et al. 2014, ApJ, 784, 53
Murakami, H., Baba, H., Barthel, P., et al. 2007, PASJ, 59, S369
Onaka, T., Matsuhara, H., Wada, T., et al. 2007, PASJ, 59, S401
Onaka, T., Matsuhara, H., Wada, T., et al. 2010, Proc. SPIE, 7731, 77310M

O15 - 8 J. Y. Seok

Onaka, T., Mori, T. I., Sakon, I., et al. 2014, ApJ, 780, 114

Peeters, E., Allamandola, L. J., Bauschlicher, C. W., Jr., et al. 2004, ApJ, 604, 252

Pendleton, Y. J., & Allamandola, L. J. 2002, ApJS, 138, 75

Pilleri, P., Joblin, C., Boulanger, F., & Onaka, T. 2015, A&A, 577, A16

Rho, J., Andersen, M., Tappe, A., et al. 2011, PAHs and the Universe, e.d. C. Joblin & A.G.G.M. Tielens (EAS Publications Series),
    46, 169

Rho, J., Onaka, T., Cami, J., & Reach, W. T. 2012, ApJL, 747, L6

Seok, J. Y., Koo, B.-C., & Onaka, T. 2012, ApJ, 744, 160

Seok, J. Y., Hirashita, H., & Asano, R. S. 2014, MNRAS, 439, 2186

Seok, J. Y., & Li, A. 2016, ApJ, 818, 2

Seok, J. Y., & Li, A. 2017, ApJ, 835, 291

Shimonishi, T., Onaka, T., Kato, D., et al. 2008, ApJL, 686, L99

Sloan, G. C., Bregman, J. D., Geballe, T. R., Allamandola, L. J., & Woodward, E. 1997, ApJ, 474, 735

Tappe, A., Rho, J., & Reach, W. T. 2006, ApJ, 653, 267

Tielens, A. G. G. M. 2008, ARA&A, 46, 289

Verstraete, L., Puget, J. L., Falgarone, E., et al. 1996, A&A, 315, L337

Vidal-Madjar, A., Lemoine, M., Ferlet, R., et al. 1998, A&A, 338, 694

Yamagishi, M., Kaneda, H., Ishihara, D., et al. 2012, A&A, 541, A10

Yang, X. J., Glaser, R., Li, A., & Zhong, J. X. 2016, MNRAS, 462, 1551